Ocean Engineering 186 (2019) 106109

Contents lists available at ScienceDirect

Ocean Engineering

journal homepage: www.elsevier.com/locate/oceaneng

Fixed-time extended state observer-based trajectory tracking and point stabilization control for marine surface vessels with uncertainties and disturbances

Jingqi Zhang, Shuanghe Yu *, Yan Yan

College of Marine Electrical Engineering, Dalian Maritime University, Dalian 116026, China

ARTICLE INFO

Keywords:
Fixed-time extended state observer (FXESO)
Trajectory tracking
Point stabilization
Marine surface vessels (MSVs)
Finite-time homogeneity control (FHC)

ABSTRACT

In this paper, a novel output feedback trajectory tracking control scheme is proposed for marine surface vessels (MSVs). A fixed-time extended state observer (FXESO) is developed to estimate unmeasured velocities and lumped disturbances, and their estimation errors converge to the origin in fixed time. Especially, the convergence time of the system is independent of the initial states of an MSV. These lumped disturbances consist of uncertainties and external time-varying disturbances. Considering control accuracy and convergence rate, a finite-time homogeneity control theory (FHC) is employed in the controller design. The proposed scheme can guarantee the tracking errors to converge to zero in finite time. Meanwhile, the point stabilization is considered as a special case of the trajectory tracking, and the superior results can be achieved under the proposed control scheme framework as well. Finally, simulation studies and comparisons demonstrate the effectiveness of the developed control scheme.

1. Introduction

In recent times, with the exploration and exploitation of marine resources, MSVs with high autonomy have attracted increasing attention for executing multiple tasks, such as pipeline inspection, military tasks, maritime surveillance, *etc.* (Srensen, 2011; Fossen, 2002; Shi et al., 2017). In order to manage to accomplish these missions or tasks, the autonomous motion control of an MSV has become a hot and crucial topic. However, the designed controllers are challenged by the adverse effects including external disturbances and uncertainties. As a consequence, it has attracted more and more attention from marine engineering and control community (Yang et al., 2019; Zhang et al., 2019; Do, 2016; Qu et al., 2018; Dai and Yu, 2018; Cui et al., 2016a).

Many remarkable control methods have been introduced for marine vessels. As an efficient control theory, sliding mode control (SMC) has been widely used for practical systems due to its rejection capacity against bounded lumped disturbances including uncertainties and disturbances (Yan and Yu, 2018; Cui et al., 2016b). However, it is worth noticing that SMC-based approaches tend to give rise to undesired high frequency oscillation (Yu et al., 2012; Tran and Kang, 2015). Consider a chattering-free control method, backstepping technique can be employed in tracking controller design (Behal et al., 2002; Yang et al., 2014). It should be pointed out that external disturbances have not been considered in spite of the desirable results being achieved in Behal et al. (2002). Recently, to compensate complex unknowns pertaining to an MSV system, intelligent control algorithms have been developed via adaptive neural networks and fuzzy logic systems (Cui et al., 2017b; Peng et al., 2013; Zhang and Zhang, 2014; Yu et al., 2017; Xiang et al., 2017; Yan and Wang, 2012; Liu et al., 2015, 2017). These innovative schemes are mainly motivated by intelligent approximators.

It is worth noting that only exponential or asymptotic convergence can be guaranteed in the aforementioned schemes. Consider the convergence rate and robustness against external disturbances and uncertainties, the finite-time control has been intensively proposed (Yu et al., 2005; Yu and Long, 2015; Li et al., 2015; Hong et al., 2002; Du and Li, 2012). In these respects, some finite-time methods have been also investigated in MSVs motion control. In Wang et al. (2017b, 2016, 2017a,b) finite-time nonsingular terminal SMC, a finite-time adding a power integrator control as well as an FHC are proposed for trajectory tracking of an MSV, respectively. Meanwhile, their tracking errors can converge to the origin rather than a small region in finite time. As known from the above papers, all states can be available, namely, state feedback is allowed. Sometimes, consider weight and cost, or sensor failures, most velocities are unmeasurable in practical applications (Fu and Yu, 2018). Therefore, it is necessary to propose an output feedback control law that only relies on positions and heading angle.

* Corresponding author.
E-mail addresses: jingqi@dlmu.edu.cn (J. Zhang), shuanghe@dlmu.edu.cn (S. Yu), y.yan@dlmu.edu.cn (Y. Yan).

https://doi.org/10.1016/j.oceaneng.2019.05.078
Received 4 January 2019; Received in revised form 28 March 2019; Accepted 31 May 2019
Available online 13 June 2019
0029-8018/

According to Wang et al. (2017b), the lumped disturbances are defined as external/internal disturbances, and anything that is difficult to model or deal with. In recent years, many researchers have devoted efforts to designing disturbance observers (DOs) such as a new linear DO (Ding et al., 2019), an exponential DO (Yang et al., 2014), a sliding mode DO (Hall and Shtessel, 2006), finite-time DOs (Wang et al., 2017b, 2016, 2017a), a linear ESO (LESO) (Cui et al., 2010, 2017a), a finite-time ESO (FTESO) (Zhao et al., 2017) *etc*. They have been extensively and widely applied in various industrial fields, such as MSV systems, autonomous underwater vehicle systems, reusable launch vehicles, *etc.* In spite of finite-time DOs or ESOs providing high estimation precision and fast convergence rate, the convergence time is dependent on the initial conditions. In Huang et al. (2019), Ni et al. (2018), Basin et al. (2017), Yu et al. (2018), Basin et al. (2016) and Sun et al. (2018), the fixed-time DOs that provide a transition time independent on the initial values are proposed, respectively. In Tian et al. (2017), a novel fixed-time state observer is presented. Consider unavailable velocities and lumped disturbances, an FXESO (Zhang et al., 2018) is developed. However, it is emphasized that the gain number and structure of the FXESO need to be improved. As such, inspired by the above analyses, an FXESO needs to be redesigned so as to provide the superior performance.

Additionally, to the best of our knowledge, there are no results on the FXESO-based finite-time output feedback control. Accordingly, motivated by these, we will intensively solve accurate tracking and stabilization problem of an MSV with uncertainties and unknown external disturbances. The major contributions of this paper are summarized as follows.

i. An FXESO is proposed to estimate the lumped disturbances and unmeasured velocities in fixed time. Compared with Basin et al. (2016), a discontinuous term $Ysign(x)$ is introduced to compensate the bounded lumped disturbances. In addition, based on the FXESO, we also design the controller rather than a single observer. Compared with Wang et al. (2016, 2017b,a) and Yang et al. (2014), the proposed FXESO can simultaneously estimate the lumped disturbances and unmeasured velocities. Compared with Wang et al. (2016, 2017b,a), Yang et al. (2014), Cui et al. (2010) and Zhao et al. (2017), the estimation errors are able to converge to the origin in fixed time which is independent on the initial states. Compared with LESO (Cui et al., 2010) and FTESO (Zhao et al., 2017), the proposed FXESO's convergence rate and accuracy are superior to both. Compared with Zhang et al. (2018), it achieves a more concise structure with much fewer parameters and obtains better performance.

ii. An FXESO-based output feedback FHC scheme is applied to trajectory tracking and point stabilization of an MSV. Compared with Wang et al. (2017a,b, 2016), in addition to the finite-time stability analysis on $t \geq T_1$, the finite-time boundness is also proven on $t < T_1$, that is to say, the system states cannot escape to the infinity in T_1, where T_1 is the fixed settling time of FXESO.

This paper is organized as follows. Section 2 presents some notations and useful preliminaries. Section 3 introduces the mathematical models of an MSV, and the control problem is set up. Section 4 proposes an FXESO-based FHC scheme under uncertainties and unknown disturbances. Section 5 demonstrates the effectiveness and superiority of the proposed scheme by simulations and comparisons. Section 6 summarizes conclusions and future works.

2. Notations and preliminaries

2.1. Notations

1. For a vector $\{\bullet\}$, $\|\bullet\|_2$ is the Euclidean 2-norm. $\{\bullet\}^T$ denotes the transpose of a matrix $\{\bullet\}$

2. $\lambda_{\min}\{\bullet\}$ and $\lambda_{\max}\{\bullet\}$ are respectively defined as the minimum and maximum eigenvalues of a matrix $\{\bullet\}$.

3. Define $x=[x_1, x_2, \dots, x_n]^T \in \mathfrak{R}^n$, $sig^\alpha(x) = [sig^\alpha(x_1), sig^\alpha(x_2), \dots, sig^\alpha(x_n)]^T$, where $sig^\alpha(x_i) = \text{sgn}(x_i)|x_i|^\alpha (i = 1, 2, \dots, n)$, $x_i \in \mathfrak{R}$, $\alpha \in (0, 1)$. $\text{sgn}(\bullet)$ is a signum function, and given by

$$\text{sgn}(x) = \begin{cases} -1, & if \quad x < 0 \\ 0, & if \quad x = 0 \\ 1, & if \quad x > 0 \end{cases} \tag{1}$$

2.2. Preliminaries

Consider a nonlinear system (Wang et al., 2017a)

$$\dot{x}(t) = f(x(t)), x(0) = 0, f(0) = 0, x \in U_0 \subset \mathfrak{R}^n \tag{2}$$

where $x = [x_1, x_2, \dots, x_n]^T$.

Definition 1 (*Wang et al., 2017a*)**.** If there exists a function $V(x)$ satisfying the following three aspects, the equilibrium $x_e = 0$ of the system (2) is globally asymptotically stable (GAS).

(i) $\dot{V}(x) \leq 0$ and $V(0) = 0$;
(ii) $V(x) > 0$ $(x \neq 0)$ is radically unbounded;
(iii) $\dot{V}(x)$ does not vanish identically along any trajectory in $\mathfrak{R}^n$, other than the null solution $x = 0$.

Definition 2 (*Hong et al., 2002; Wang et al., 2017a*)**.** Denote $V(x)$: $\mathfrak{R}^n \to \mathfrak{R}$ be a continuous function. $V(x)$ is said to be homogeneous of degree $\sigma > 0$ with respect to weights $(r_1, r_2, \dots r_n)$, where $r_i > 0$, $i = 1, 2, 3, \dots, n$. If, for any given $\varepsilon > 0$, $V(\varepsilon^{r_1}x_1, \varepsilon^{r_2}x_2, \dots, \varepsilon^{r_n}x_n) = \varepsilon^\sigma V(x)$, $\forall x \in \mathfrak{R}^n$.

Let $f(x) = [f_1(x), f_2(x), \dots, f_n(x)]^T$ be a continuous vector field. $f(x)$ is said to be homogeneous of degree $k \in \mathfrak{R}$ with respect to weights $(r_1, r_2, \dots r_n)$. If for any given $\varepsilon > 0$, $f_i(\varepsilon^{r_1}x_1, \varepsilon^{r_2}x_2, \dots, \varepsilon^{r_n}x_n) = \varepsilon^{r_i+k}f_i(x)$, $i = 1, 2, \dots, n$, $\forall x \in \mathfrak{R}^n$. The system (2) is said to be homogeneous if $f(x)$ is homogeneous.

Lemma 1 (*Wang et al., 2017b*)**.** *Consider the system (2), a continuous positive definite function $V(x) : D \to \mathfrak{R}$, if there exist $\dot{V}(x) + c(V(x))^\sigma \leq 0$ $(c > 0, \sigma \in (0, 1))$ and $x \in \upsilon \setminus \{0\}$, then the origin is a finite-time stable equilibrium of the system (2), where $\upsilon \subset D$ is an open neighborhood of the origin. Furthermore, the setting-time function T is expressed as*

$$T(x) \leq \frac{1}{c(1-\sigma)}(V(x))^{1-\sigma}$$

If $D = \mathfrak{R}^n$, $V(x)$ is proper, and $\dot{V}(x) < 0$ on $\mathfrak{R}^n \setminus \{0\}$, then the origin is a globally finite-time-stable (GFTS) equilibrium of the system (2)

Lemma 2 (*Hong et al. (2002)*)**.** *The system (2) is GFTS if it is GAS and is homogeneous of degree $k < 0$.*

3. System modeling and problem formulation

From Fig. 1, two coordinate systems are commonly defined.

The 3-DOF MSV models can be expressed as Wang et al. (2017a)

$$\begin{cases} \dot{\eta} = R(\psi)\upsilon \\ M\dot{\upsilon} + C(\upsilon)\upsilon + D(\upsilon)\upsilon = \tau + b \end{cases} \tag{3}$$

where the motions in heave, pitch and roll are neglected. The vector $\eta = [x, y, \psi]^T$ is the locations and yaw angle. The $\upsilon = [u, v, r]^T$ is velocity vector including surge velocity u, sway velocity v as well as yaw angle velocity r. The vectors $\tau = [\tau_1, \tau_2, \tau_3]^T$ and $b(t) = [b_1(t), b_2(t), b_3(t)]^T$ are respectively control input and unknown environmental disturbance. The rotation matrix $R(\psi)$ is given by

$$R(\psi) = \begin{bmatrix} \cos(\psi) & -\sin(\psi) & 0 \\ \sin(\psi) & \cos(\psi) & 0 \\ 0 & 0 & 1 \end{bmatrix} \tag{4}$$

with the following properties:

$$\dot{R}(\psi) = R(\psi)S(r) \tag{5}$$

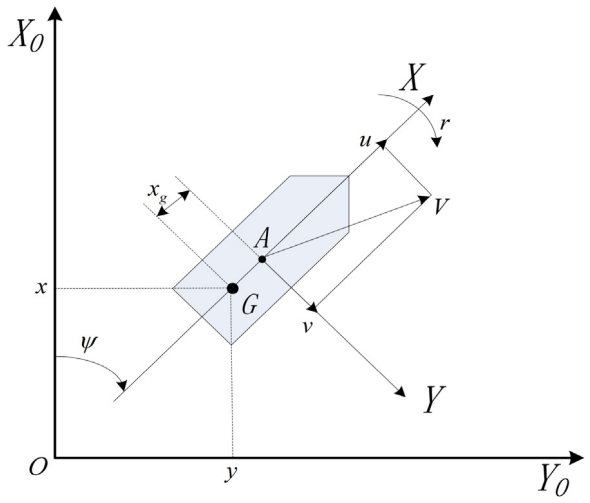

Fig. 1. Definition of the earth-fixed OX_0Y_0 and the body-fixed AXY coordinate frames.

$$R^T(\psi)S(r)R(\psi) = R(\psi)S(r)R^T(\psi) = S(r) \tag{6}$$

$$S(r) = \begin{bmatrix} 0 & -r & 0 \\ r & 0 & 0 \\ 0 & 0 & 0 \end{bmatrix} \tag{7}$$

$$R^T(\psi)R(\psi) = I \quad and \quad \|R(\psi)\| = 1 \tag{8}$$

Assumption 1.

(1). The smooth reference trajectory η_d has the bounded first and second derivatives, i.e.,$\dot{\eta}_d$, $\ddot{\eta}_d$.

(2). $C(v)$ and $D(v)$ are unmodeled dynamics.

(3). The disturbance vector b imposed on the MSVs satisfies $\|\dot{b}(t)\| \leq \varepsilon$, where ε is an unknown nonnegative bounded constant.

(4). The velocity vector $v = [u, v, r]^T$ is unavailable.

In this paper, our objective is to design an FXESO-based FHC scheme under uncertainties and unknown disturbances so as to track η_d and v_d accurately in finite time. Meanwhile, under the same control framework, an MSV can be stabilized to a desired locations and yaw angle.

4. FXESO-Based FHC trajectory tracking and point stabilization control

The structure of the MSV control system is listed in Fig. 2.

4.1. Coordinate transformation

Coordinate transformation can be considered on v and v_d, and given by

$$\begin{cases} w = R(\psi)v \\ w_d = R(\psi_d)v_d \end{cases} \tag{9}$$

where $w = [w_1, w_2, w_3]^T$, $w_d = [w_{d1}, w_{d2}, w_{d3}]^T$.

Together with (3) and (9), using properties (5)–(8), we have

$$\begin{cases} \dot{\eta} = w \\ \dot{w} = R(\psi)M^{-1}\tau + \chi \\ \dot{\eta}_d = w_d \end{cases} \tag{10}$$

where $\eta_d = [x_d, y_d, \psi_d]^T$, $\chi = R(\psi)s(r)v - R(\psi)M^{-1}C(v)v - R(\psi)M^{-1}D(v)v + R(\psi)M^{-1}b$ is an unknown nonlinearity.

We have the following tracking errors

$$\begin{cases} \eta_e = \eta - \eta_d \\ w_e = w - w_d \end{cases} \tag{11}$$

Accordingly, computing the time derivative of (11), we obtain

$$\begin{cases} \dot{\eta}_e = \dot{\eta} - \dot{\eta}_d = w - w_d = w_e \\ \dot{w}_e = \dot{w} - \dot{w}_d = R(\psi)M^{-1}\tau + \chi - \dot{w}_d \end{cases} \tag{12}$$

Assumption 2. According to Wang et al. (2017b), there exists a bounded constant H_n, such that $\|\dot{\chi}\| \leq H_n$ holds.

4.2. Design of the FXESO

In this subsection, the FXESO is designed to obtain the exact estimations for the velocities and the lumped disturbances. The FXESO can be proposed as follows.

$$\begin{cases} \dot{\hat{\eta}} = \hat{w} + \mu_1 sig^{\alpha_1}(\eta - \hat{\eta}) + \varepsilon_1 sig^{\beta_1}(\eta - \hat{\eta}) \\ \dot{\hat{w}} = R(\psi)M^{-1}\tau + \hat{\chi} + \mu_2 sig^{\alpha_2}(\eta - \hat{\eta}) + \varepsilon_2 sig^{\beta_2}(\eta - \hat{\eta}) \\ \dot{\hat{\chi}} = \mu_3 sig^{\alpha_3}(\eta - \hat{\eta}) + \varepsilon_3 sig^{\beta_3}(\eta - \hat{\eta}) + \Upsilon sign(\eta - \hat{\eta}) \end{cases} \tag{13}$$

where $\alpha_i \in (0, 1)$, $\beta_i > 1$, $i = 1, 2, 3$. $\alpha_i = i\bar{\alpha} - (i - 1)$, $\beta_i = i\bar{\beta} - (i - 1)$, $\bar{\alpha} \in (1 - l_1)$, $\bar{\beta} \in (1 + l_2)$ with small enough constants $l_1 > 0$, $l_2 > 0$, $H_n < \Upsilon$. The FXESO gains are assigned to ensure the following matrices are Hurwitz.

$$P_1 = \begin{bmatrix} -\mu_1 & 1 & 0 \\ -\mu_2 & 0 & 1 \\ -\mu_3 & 0 & 0 \end{bmatrix}$$

$$P_2 = \begin{bmatrix} -\varepsilon_1 & 1 & 0 \\ -\varepsilon_2 & 0 & 1 \\ -\varepsilon_3 & 0 & 0 \end{bmatrix}$$

Theorem 1. *Under Assumption 2, the FXESO (13) can simultaneously estimate η, w, χ in fixed time. Moreover, the convergence time is bounded by*

$$T_1 \leq \frac{\lambda^{\vartheta}{}_{\max}(\Omega_1)}{\gamma_1 \vartheta} + \frac{1}{\gamma_2 \sigma \varpi^{\sigma}} \tag{14}$$

where $\gamma_1 = \lambda_{\min}(Q_1)/\lambda_{\max}(\Omega_1)$, $\gamma_2 = \lambda_{\min}(Q_2)/\lambda_{\max}(\Omega_2)$, $\vartheta = 1 - \bar{\alpha}$, $\sigma = \bar{\beta} - 1$. The positive constant $\varpi \leq \lambda_{\min}(\Omega_2)$. Q_1, Q_2, Ω_1 and Ω_2 are nonsingular, symmetric as well as positive definite matrices and satisfied by $\Omega_1 P_1 + P_1{}^T \Omega_1 = -Q_1$, $\Omega_2 P_2 + P_2{}^T \Omega_2 = -Q_2$.

Proof. Consider the following estimation errors

$$\begin{cases} \tilde{e}_1 = \eta - \hat{\eta} \\ \tilde{e}_2 = w - \hat{w} \\ \tilde{e}_3 = \chi - \hat{\chi} \end{cases} \tag{15}$$

Differentiating (15) with respect to time yields

$$\begin{cases} \dot{\tilde{e}}_1 = \tilde{e}_2 - \mu_1 sig^{\alpha_1}(\tilde{e}_1) - \varepsilon_1 sig^{\beta_1}(\tilde{e}_1) \\ \dot{\tilde{e}}_2 = \tilde{e}_3 - \mu_2 sig^{\alpha_2}(\tilde{e}_1) - \varepsilon_2 sig^{\beta_2}(\tilde{e}_1) \\ \dot{\tilde{e}}_3 = \dot{\chi} - \mu_3 sig^{\alpha_3}(\tilde{e}_1) - \varepsilon_3 sig^{\beta_3}(\tilde{e}_1) - \Upsilon sign(\tilde{e}_1) \end{cases} \tag{16}$$

According to Zhang et al. (2018), the following proof on the estimation errors converging with zero errors in fixed time is divided into the following two steps:

(1). We first prove the following error system (17) can converge to zero in fixed time.

$$\begin{cases} \dot{\tilde{e}}_1 = \tilde{e}_2 - \mu_1 sig^{\alpha_1}(\tilde{e}_1) - \varepsilon_1 sig^{\beta_1}(\tilde{e}_1) \\ \dot{\tilde{e}}_2 = \tilde{e}_3 - \mu_2 sig^{\alpha_2}(\tilde{e}_1) - \varepsilon_2 sig^{\beta_2}(\tilde{e}_1) \\ \dot{\tilde{e}}_3 = \dot{\chi} - \mu_3 sig^{\alpha_3}(\tilde{e}_1) - \varepsilon_3 sig^{\beta_3}(\tilde{e}_1) \end{cases} \tag{17}$$

According to Theorem 2 in Basin et al. (2016), the error vector $\tilde{e} = [\tilde{e}_1, \tilde{e}_2, \tilde{e}_3]$ can converge to the origin in fixed time.

(2). Referring to Theorem 1 in Zhang et al. (2018), once $\tilde{e}_1 = 0$ achieves after the time T_1, then $\tilde{e}_1$ will maintain in $\tilde{e}_1 = 0$ in the rest of time. Accordingly, $\tilde{e}_1 = \dot{\tilde{e}}_1 = 0$ and $\tilde{e}_2 = \tilde{e}_3 = 0$ can be obtained. Hence,

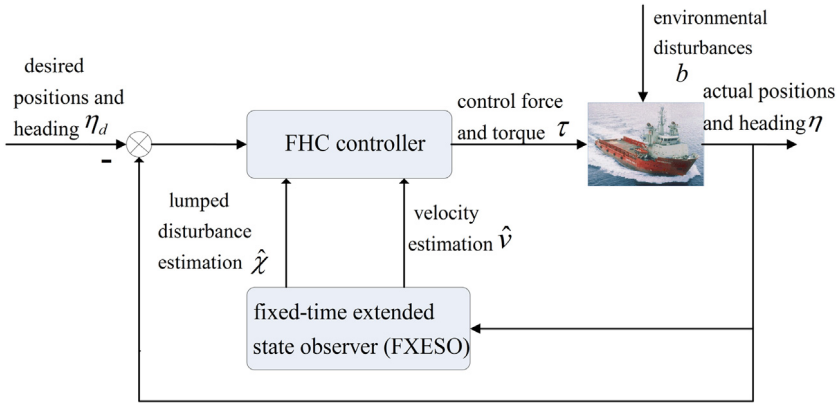

Fig. 2. The structure of the MSV control system.

there is a bounded time T_1, such that $\tilde{e}_1 = \tilde{e}_2 = \tilde{e}_3 = 0$ holds for all $t \geq T_1$. In view of Zhang et al. (2018), implying the following identity holds

$$\dot{\tilde{e}}_3 = -Y\,sign(\tilde{e}_1) + \dot{\chi} = 0, \qquad t \geq T_1 \tag{18}$$

For the lumped disturbance, it is considered to be an augmented state. Hence, the FXESO is called as an extended state observer.

Remark 1. Compared with an FXESO in Zhang et al. (2018), the gain number of the proposed observer ($\mu_1 = \varepsilon_1$, $\mu_2 = \varepsilon_2$, $\mu_3 = \varepsilon_3$, Y) is less than one (η, b, Λ, Y, T_u) in Zhang et al. (2018), where T_u is switching time. By referring to Ni et al. (2018), the design parameter T_u is typically selected through trial and error. Therefore, the selection of T_u will affect the estimation performance and it is not prone to adjust. Note that the proposed FXESO in this paper can achieve a more concise structure with much fewer parameters and obtain better performances. According to Zhang et al. (2018), $Y\tanh(x) = Y(e^x - e^{-x})/(e^x + e^{-x})$ can replace $Y\,sign(x)$ so as to reduce the chattering of the FXESO.

4.3. Design of the FXESO-based FHC

In this subsection, the FXESO-based output feedback FHC is proposed as follows

$$\tau = M\,R(\psi)^{-1}[-k_1 sig^{\gamma_1}(\eta_e) - k_2 sig^{\gamma_2}(\hat{e}_2) - \hat{\chi} + \dot{w}_d] \tag{19}$$

where $\hat{e}_2 = \hat{w} - w_d$. $k_1 > 0$, $k_2 > 0$, $0 < \gamma_1 < 1$, $\gamma_2 = 2\gamma_1/(1+\gamma_1)$.

Theorem 2. *Under Assumptions 1–2, the control law (19) can make an MSV track the reference trajectory accurately, and the tracking errors can converge with zero errors in finite time after the exact estimations for the velocities and lumped disturbances, i.e., $\hat{\eta}(t) \equiv \eta(t) \equiv \eta_d(t)$, $\hat{w}(t) \equiv w_d(t)$.*

Proof.

Firstly, we will prove η_{ei}, $\tilde{e}_{2i}$ and $\tilde{e}_{3i}$ do not escape to the infinity on $[0, T_1)$.

A bounded function is chosen as

$$B\left(\eta_{ei}, \tilde{e}_{2i}, \tilde{e}_{3i}\right) = \frac{1}{2}(\eta_{ei}^2 + \tilde{e}_{2i}^2 + \tilde{e}_{3i}^2) \tag{20}$$

where $i = 1, 2, 3$ represent x, y, ψ, respectively.

Due to $\hat{w}_{ei} + \tilde{e}_{2i} = w_{ei} = \dot{\eta}_{ei}$ and $|\dot{\chi}_i| \leq H_n < Y$, computing the derivative of (20), we have

$$\dot{B}\left(\eta_{ei}, \tilde{e}_{2i}, \tilde{e}_{3i}\right) = \eta_{ei}\cdot\dot{\eta}_{ei} + \tilde{e}_{2i}\cdot\dot{\tilde{e}}_{2i} + \tilde{e}_{3i}\cdot\dot{\tilde{e}}_{3i} = \eta_{ei}\cdot\left(\hat{w}_{ei} + \tilde{e}_{2i}\right) + \tilde{e}_{2i}\cdot\dot{\tilde{e}}_{2i} + \tilde{e}_{3i}\cdot\dot{\tilde{e}}_{3i} \tag{21}$$

In the light of $\begin{cases} \dot{\tilde{e}}_{2i} = \tilde{e}_{3i} - \mu_2 sig^{\alpha_2}(\tilde{e}_{1i}) - \varepsilon_2 sig^{\beta_2}(\tilde{e}_{1i}) \\ \dot{\tilde{e}}_{3i} = \dot{\chi}_i - \mu_3 sig^{\alpha_3}(\tilde{e}_{1i}) - \varepsilon_3 sig^{\beta_3}(\tilde{e}_{1i}) - Y\,sign(\tilde{e}_{1i}) \end{cases}$.

Therefore, (21) is rewritten as follows

$$\begin{aligned}\dot{B}\left(\eta_{ei}, \tilde{e}_{2i}, \tilde{e}_{3i}\right) = {} & \eta_{ei}\cdot\left(\hat{w}_{ei} + \tilde{e}_{2i}\right) + \tilde{e}_{2i}\cdot\left[\tilde{e}_{3i} - \mu_2 sig^{\alpha_2}(\tilde{e}_{1i}) - \varepsilon_2 sig^{\beta_2}(\tilde{e}_{1i})\right] \\ & + \tilde{e}_{3i}\cdot\left[\dot{\chi}_i - \mu_3 sig^{\alpha_3}(\tilde{e}_{1i}) - \varepsilon_3 sig^{\beta_3}(\tilde{e}_{1i}) - Y\,sign(\tilde{e}_{1i})\right]\end{aligned} \tag{22}$$

Accordingly

$$\begin{aligned}\dot{B}\left(\eta_{ei}, \tilde{e}_{2i}, \tilde{e}_{3i}\right) \leq {} & \eta_{ei}\cdot\hat{w}_{ei} + \eta_{ei}\cdot\tilde{e}_{2i} + \tilde{e}_{2i}\cdot\tilde{e}_{3i} + 2\cdot Y\cdot\left|\tilde{e}_{3i}\right| - \tilde{e}_{2i}\cdot\mu_2 sig^{\alpha_2}(\tilde{e}_{1i}) \\ & - \tilde{e}_{2i}\cdot\varepsilon_2 sig^{\beta_2}(\tilde{e}_{1i}) - \tilde{e}_{3i}\cdot\mu_3 sig^{\alpha_3}(\tilde{e}_{1i}) - \tilde{e}_{3i}\cdot\varepsilon_3 sig^{\beta_3}(\tilde{e}_{1i})\end{aligned} \tag{23}$$

Let

$$H = -\tilde{e}_{2i}\cdot\mu_2 sig^{\alpha_2}(\tilde{e}_{1i}) - \tilde{e}_{2i}\cdot\varepsilon_2 sig^{\beta_2}(\tilde{e}_{1i}) - \tilde{e}_{3i}\cdot\mu_3 sig^{\alpha_3}(\tilde{e}_{1i}) - \tilde{e}_{3i}\cdot\varepsilon_3 sig^{\beta_3}(\tilde{e}_{1i}) \tag{24}$$

Since $\tilde{e}_{1i}, \tilde{e}_{2i}, \tilde{e}_{3i}$ can converge with zero errors in fixed time, then $\tilde{e}_{1i}, \tilde{e}_{2i}, \tilde{e}_{3i}$ are bounded, respectively, that is, $|H| \leq L_2$.

Considering the Mean Inequality, we obtain

$$\begin{aligned}\dot{B}\left(\eta_{ei}, \tilde{e}_{2i}, \tilde{e}_{3i}\right) \leq {} & \frac{1}{2}\eta_{ei}^2 + \frac{1}{2}\hat{w}_{ei}^2 + \frac{1}{2}\eta_{ei}^2 + \frac{1}{2}\tilde{e}_{2i}^2 + \frac{1}{2}\tilde{e}_{2i}^2 + \frac{1}{2}\tilde{e}_{3i}^2 + 2Y^2 + \frac{1}{2}\tilde{e}_{3i}^2 + L_2 \\ = {} & \eta_{ei}^2 + \tilde{e}_{2i}^2 + \tilde{e}_{3i}^2 + \frac{1}{2}\hat{w}_{ei}^2 + 2Y^2 + L_2\end{aligned} \tag{25}$$

Since $\hat{w}_{ei}$ is also bounded, that is to say, $|\hat{w}_{ei}| \leq L_3$

Therefore

$$\dot{B}\left(\eta_{ei}, \tilde{e}_{2i}, \tilde{e}_{3i}\right) \leq \eta_{ei}^2 + \tilde{e}_{2i}^2 + \tilde{e}_{3i}^2 + \frac{1}{2}L_3^2 + 2Y^2 + L_2 \tag{26}$$

Let $\bar{L} = \frac{1}{2}L_3^2 + 2Y^2 + L_2$

Hence, we have

$$\dot{B}\left(\eta_{ei}, \tilde{e}_{2i}, \tilde{e}_{3i}\right) \leq \eta_{ei}^2 + \tilde{e}_{2i}^2 + \tilde{e}_{3i}^2 + \bar{L} = 2B\left(\eta_{ei}, \tilde{e}_{2i}, \tilde{e}_{3i}\right) + \bar{L} \tag{27}$$

Then, the above inequality is solved as

$$B\left(\eta_{ei}, \tilde{e}_{2i}, \tilde{e}_{3i}\right) \leq \left(B\left(\eta_{ei}(0), \tilde{e}_{2i}(0), \tilde{e}_{3i}(0)\right) + \left(\bar{L}/2\right)\right)e^{2t} - \left(\bar{L}/2\right) \tag{28}$$

As shown from (28), for $\forall t \leq T_1$, η_{ei}, $\tilde{e}_{2i}$ and $\tilde{e}_{3i}$ are bounded. Therefore, we can conclude that the system states do not escape to the infinity.

For $t \geq T_1$, substituting the control law (19) into the tracking errors (12), and together with $\hat{e}_1 = \hat{\eta} - \eta_d = \eta - \eta_d$ and $\hat{e}_2 = \hat{w} - w_d$, the following formula can be obtained

$$\begin{cases} \dot{\hat{e}}_1 = \hat{e}_2 \\ \dot{\hat{e}}_2 = -k_1 sig^{\gamma_1}(\hat{e}_1) - k_2 sig^{\gamma_2}(\hat{e}_2) \end{cases} \tag{29}$$

The following Lyapunov function is constructed as:

$$V(\hat{e}_1, \hat{e}_2) = \sum_i^3 (k_1 \int_0^{\hat{e}_{i1}} sig^{\gamma_1}(\mu)d\mu + \frac{1}{2}\hat{e}_{i2}^2) \tag{30}$$

where $i = 1, 2, 3$.

We can obtain the following derivative of (30) along the system (29)

$$\begin{aligned}\dot{V}(\hat{e}_1,\hat{e}_2) &= k_1\sum_i^n sig^{\gamma_1}(\hat{e}_{i1})\hat{e}_{i2}\\ &\quad-\sum_i^n \hat{e}_{i2}(k_1 sig^{\gamma_1}(\hat{e}_{i1})+k_2 sig^{\gamma_2}(\hat{e}_{i2}))\\ &= -k_2\sum_i^n \hat{e}_{i2}sig^{\gamma_2}(\hat{e}_{i2})\\ &= -k_2\sum_i^n |\hat{e}_{i2}|^{1+\gamma_2}\end{aligned} \tag{31}$$

(31) implies $V(\hat{e}_1,\hat{e}_2)$ is monotonically decreasing, that is, $V(\hat{e}_1,\hat{e}_2)\le V(\hat{e}_1(0),\hat{e}_2(0))$, then $\hat{e}_1(t)$ and $\hat{e}_2(t)$ are bounded. Note that $\ddot{V}=-k_2(1+\gamma_2)\hat{e}_2^{\gamma_2}sig^{\gamma_2}(\hat{e}_2)$ is also bounded, then $\dot{V}$ is uniformly continuous. Taking advantage of Barbalat's Lemma, we obtain $\lim_{t\to\infty}\dot{V}=0$, that is, $\lim_{t\to\infty}\hat{e}_2=0$.

The derivative of $\hat{e}_{i1}\hat{e}_{i2}$ along the system (29) is given by

$$\frac{d}{dt}(\hat{e}_{i1}\hat{e}_{i2}) = -k_1\hat{e}_{i1}sig^{\gamma_1}(\hat{e}_{i1})-k_2\hat{e}_{i1}sig^{\gamma_2}(\hat{e}_{i2})+\hat{e}_{i2}^2 \tag{32}$$

Let $H_1=-k_2\hat{e}_{i1}sig^{\gamma_2}(\hat{e}_{i2})+\hat{e}_{i2}^2$, $H_2=-k_1\hat{e}_{i1}sig^{\gamma_1}(\hat{e}_{i1})$. Taking the time derivative of H_2 yields

$$\dot{H}_2=-k_1[\hat{e}_{i2}sig^{\gamma_1}(\hat{e}_{i1})+\gamma_1 sig^{\gamma_1}(\hat{e}_{i1})\hat{e}_{i2}] \tag{33}$$

From (33), $\dot{H}_2$ is bounded. Hence, we can conclude H_2 is uniformly continuous. Together with $\lim_{t\to\infty}\hat{e}_2=0$, then $\lim_{t\to\infty}H_1=0$. According to Lemma 2 in Du and Li (2012), $\lim_{t\to\infty}H_2=0$, so $\lim_{t\to\infty}\hat{e}_1=0$. Hence, the system (29) is GAS.

It is worth noticing that a negative degree $k=(\gamma_1-1)/2<0$ with respect to the dilation $(r_1,r_2)=(1,\frac{1+\gamma_1}{2})$, the system (29) can be rewritten as

$$\begin{cases} f_1(\varepsilon^{r_1}\hat{e}_{i1},\varepsilon^{r_2}\hat{e}_{i2})=\varepsilon^{k+r_1}f_1(\hat{e}_{i1},\hat{e}_{i2})\\ f_2(\varepsilon^{r_1}\hat{e}_{i1},\varepsilon^{r_2}\hat{e}_{i2})=\varepsilon^{k+r_2}f_2(\hat{e}_{i1},\hat{e}_{i2})\end{cases} \tag{34}$$

Considering Lemma 2, the system (29) can be confirmed to be GFTS.

Remark 2. Compared with observer-based control schemes such as Wang et al. (2017a,b, 2016), the proposed scheme's stability analysis in $t<T_1$ is proven.

Additionally, the point stabilization is considered as a special case of the trajectory tracking, so the desired η_d is a constant value, i.e., $\dot{\eta}_d=w_d=0$. Hence, the following point stabilization control law can be obtained

$$\tau = MR(\psi)^{-1}[-k_1 sig^{\gamma_1}(\eta_e)-k_2 sig^{\gamma_2}(\iota\hat{w})-\hat{\chi}] \tag{35}$$

5. Simulation and comparison studies

5.1. FXESO-Based FHC trajectory tracking performance

In this subsection, the FXESO-based FHC trajectory tracking performance will be demonstrated and carried out on CyberShip II. The parameters of the vessel can refer to Yang et al. (2014).

In control law (19), if $\gamma_1=\gamma_2=1$, then the FHC will be transformed into a traditional asymptotic one. The control performance of the above two controllers will be compared in the following simulations. Note that $\chi=R(\psi)s(r)v-R(\psi)M^{-1}C(v)v-R(\psi)M^{-1}D(v)v+R(\psi)M^{-1}b$ is considered as the lumped disturbances.

In the simulations, the initial values for the FXESO can be selected as $\hat{\eta}(0)=[0.5,0.5,\pi/3]^T$, $\iota\hat{w}(0)=[0,0,0]^T$, $\hat{\chi}(0)=[0,0,0]^T$, respectively. The FXESO gains are chosen as $\mu_1=\varepsilon_1=5$, $\mu_2=\varepsilon_2=20$, $\mu_3=\varepsilon_3=50$. Additionally, $\bar{\alpha}=0.8$, $\bar{\beta}=1.2$, so $\alpha_1=0.8$, $\alpha_2=0.6$, $\alpha_3=0.4$, $\beta_1=1.2$, $\beta_2=1.4$, $\beta_3=1.6$. The controller gains are selected as $k_1=0.07$, $k_2=0.17$, $\gamma_1=0.3$, $\gamma_2=0.5$. The initial conditions for CyberShip II are considered as $\eta(0)=[0.5,0.5,\pi/3]^T$, $v(0)=[0,0,0]^T$, $w(0)=[0,0,0]^T$.

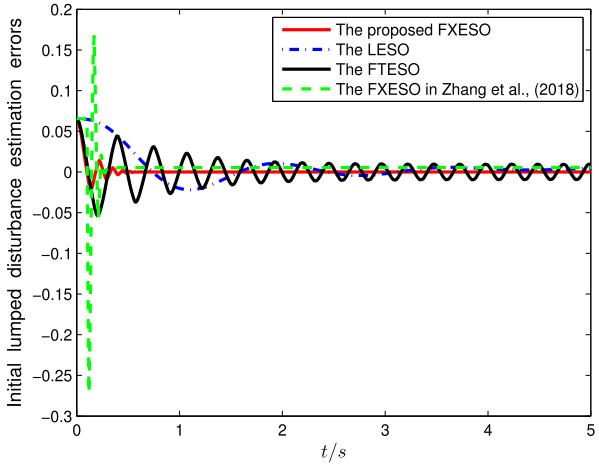

Fig. 3. The initial lumped disturbance estimation errors in surge.

The reference trajectory and disturbance vector, which refer to Yang et al. (2014), are given by

$$\eta_d=\begin{bmatrix}4\sin(0.02t)\\ 2.5(1-\cos(0.02t))\\ 0.02t\end{bmatrix}$$

$$b=\begin{bmatrix}1.3+2.0\sin(0.02t)+1.5\sin(0.1t)\\ -0.9+2.0\sin(0.02t-\pi/6)+1.5\sin(0.3t)\\ -\sin(0.09t+\pi/3)-4\sin(0.01t)\end{bmatrix}$$

In order to verify the proposed FXESO's performance, it is compared with the following FTESO (36), LESO (37) and FXESO (38) in Zhang et al. (2018), and the simulation results are plotted in Figs. 3–8. Meanwhile, their quantitative analyses are summarized in Table 1. It can be seen that the performance of the proposed FXESO is obviously superior to FTESO (36), LESO (37) and FXESO (38) in Zhang et al. (2018).

$$\begin{cases}\dot{\hat{\eta}}=\iota\hat{w}-\kappa_1 sig^{(\frac{\alpha+1}{2})}(\hat{\eta}-\eta)\\ \iota\dot{\hat{w}}=\hat{\chi}-\kappa_2 sig^{(\frac{\alpha+1}{2})}(\hat{\eta}-\eta)+R(\psi)M^{-1}\tau\\ \dot{\hat{\chi}}=-\kappa_3 sig^{\alpha}(\hat{\eta}-\eta)\end{cases} \tag{36}$$

where $\kappa_1=5$, $\kappa_2=20$, $\kappa_3=50$, $\alpha=0.4$.

$$\begin{cases}\dot{\hat{\eta}}=\iota\hat{w}+\nu_1(\eta-\hat{\eta})\\ \iota\dot{\hat{w}}=\hat{\chi}+\nu_2(\eta-\hat{\eta})+R(\psi)M^{-1}\tau\\ \dot{\hat{\chi}}=\nu_3(\eta-\hat{\eta})\end{cases} \tag{37}$$

where $\nu_1=5$, $\nu_2=20$, $\nu_3=50$.

In Zhang et al. (2018), the FXESO is given by

$$\begin{cases}\dot{Z}_1=Z_2+e^{\eta+b}\Lambda sig^{\alpha_1}(x_1-Z_1)+e^{\eta+b}(1-\Lambda)sig^{\beta_1}(x_1-Z_1)\\ \dot{Z}_2=Z_3+e^{2\eta+b}\Lambda sig^{\alpha_2}(x_1-Z_1)+e^{2\eta+b}(1-\Lambda)sig^{\beta_2}(x_1-Z_1)+BU\\ \dot{Z}_3=Z_3+e^{3\eta+b}\Lambda sig^{\alpha_3}(x_1-Z_1)+e^{3\eta+b}(1-\Lambda)sig^{\beta_3}(x_1-Z_1)\\ \qquad+Ysign(x_1-Z_1)\end{cases} \tag{38}$$

where $Y=2$, $b=1.4$, $\eta=1.75$, $T_u=0.1$.

In Table 1, the FXESO (13) is the proposed extended state observer in this paper, and the FXESO (38) is in Zhang et al. (2018). $\iota\hat{w}_{ei}(i=1,2,3)$ is the velocity estimation error between the actual and estimated velocity. $\hat{\chi}_{ei}(i=1,2,3)$ is the lumped disturbance estimation error between the actual and estimated lumped disturbance. The transient and steady-state performance can be evaluated by the integrated time absolute error (ITAE=$\int_0^t t\,|e(\delta)|d\delta$), the integrated absolute error

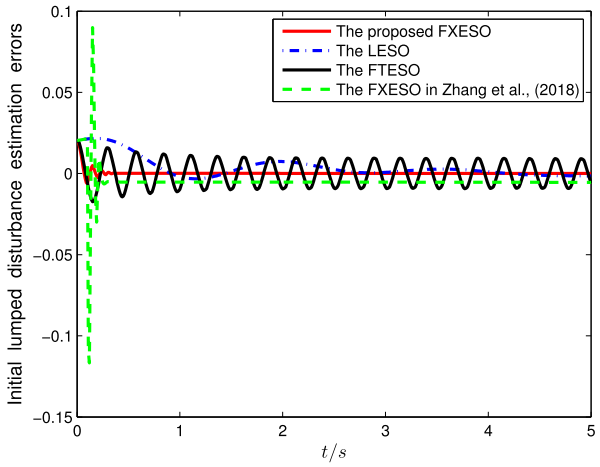

Fig. 4. The initial lumped disturbance estimation errors in sway.

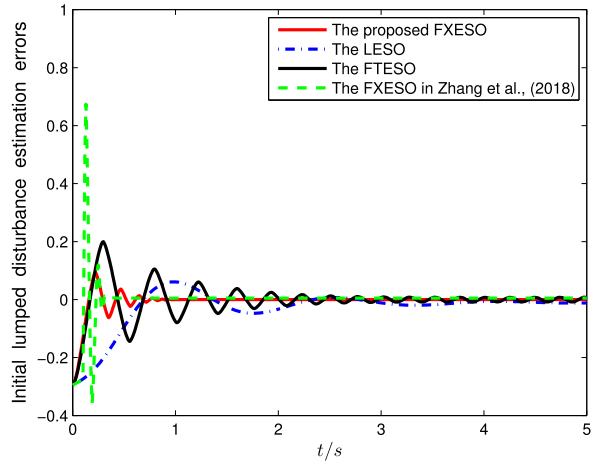

Fig. 5. The initial lumped disturbance estimation errors in yaw.

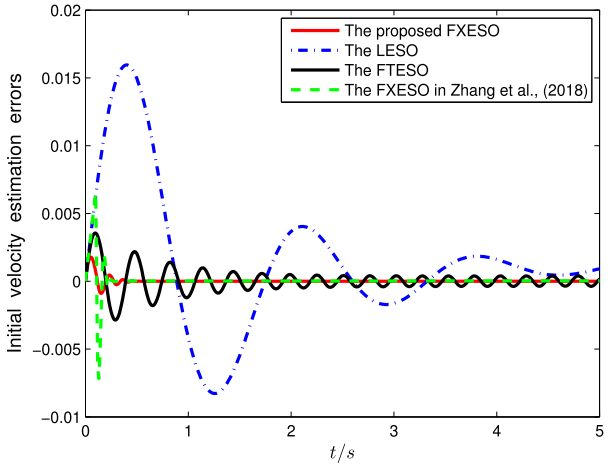

Fig. 6. The initial velocity estimation errors in surge.

(IAE=$\int_0^t |e(\delta)|d\delta$) as well as the settling time. For Table 1, the selection criteria for the settling time is based on the lumped disturbance errors within the range of 0.001. t_{final} is the running time of the simulation, i.e., $t_{final} = 300$ s.

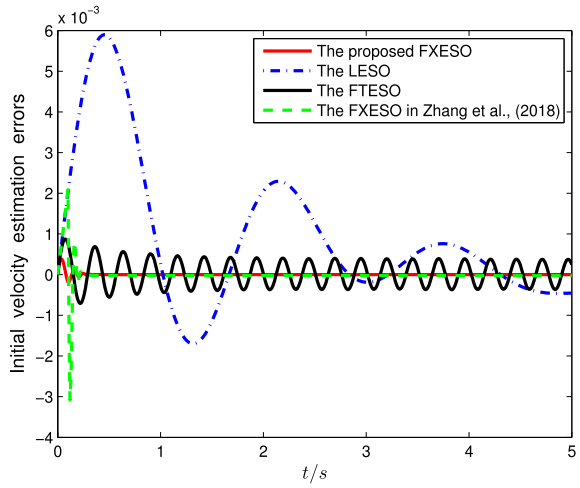

Fig. 7. The initial velocity estimation errors in sway.

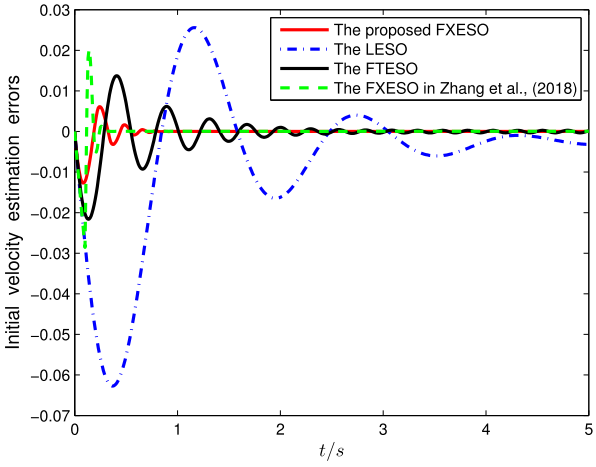

Fig. 8. The initial velocity estimation errors in yaw.

Table 1
Performance indices comparisons of observers.

Observer	FXESO (13)	LESO (37)	FTESO (36)	FXESO (38)
Settling time t_s	0.93	–	–	–
$\int_0^{t_{final}} \lvert\hat{w}_{e1}\rvert dt$	$2.7539 * 10^{-4}$	0.2146	0.0748	0.0311
$\int_0^{t_{final}} \lvert\hat{w}_{e2}\rvert dt$	$8.1944 * 10^{-5}$	0.1962	0.0734	0.0306
$\int_0^{t_{final}} \lvert\hat{w}_{e3}\rvert dt$	0.0029	0.6984	0.0342	0.0332
$\int_0^{t_{final}} \lvert\hat{\chi}_{e1}\rvert dt$	0.0197	0.8407	1.8294	4.3048
$\int_0^{t_{final}} \lvert\hat{\chi}_{e2}\rvert dt$	0.0143	0.7788	1.8087	4.2927
$\int_0^{t_{final}} \lvert\hat{\chi}_{e3}\rvert dt$	0.1036	2.7427	0.6000	4.3526
$\int_0^{t_{final}} t\lvert\hat{w}_{e1}\rvert dt$	0.0076	29.9312	11.0018	4.5666
$\int_0^{t_{final}} t\lvert\hat{w}_{e2}\rvert dt$	0.0069	28.2342	10.9943	4.5665
$\int_0^{t_{final}} t\lvert\hat{w}_{e3}\rvert dt$	0.0575	98.2486	2.7752	4.5657
$\int_0^{t_{final}} t\lvert\hat{\chi}_{e1}\rvert dt$	1.9970	119.2989	271.0162	643.2594
$\int_0^{t_{final}} t\lvert\hat{\chi}_{e2}\rvert dt$	1.8516	112.6380	270.9653	643.2576
$\int_0^{t_{final}} t\lvert\hat{\chi}_{e3}\rvert dt$	9.3236	392.7787	48.1569	643.1312

The FXESO-based FHC simulation results are shown in Figs. 9–13. The velocity tracking errors for two schemes in the body-fixed and earth-fixed frame are plotted in Figs. 9–10. The locations and yaw angle tracking errors are represented in Fig. 11. As can be seen from Figs. 9–11, the tracking performance of the proposed scheme is superior to the asymptotic scheme in convergence rate and control accuracy. The control inputs, as shown in Fig. 12, reveal that the force and torque acting on CyberShip II are smooth and reasonable. From Fig. 13, it is

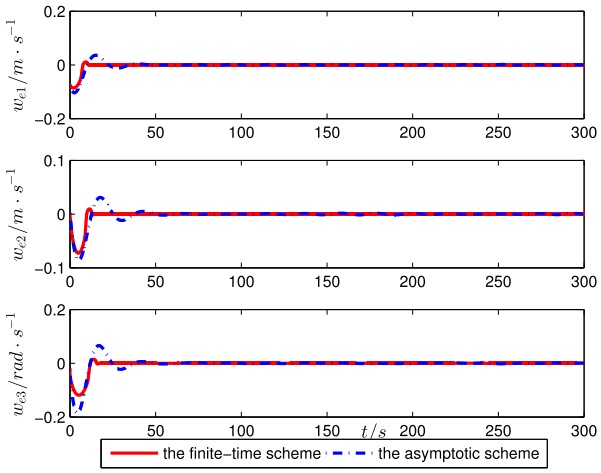

Fig. 9. The velocity tracking errors in the body-fixed frame.

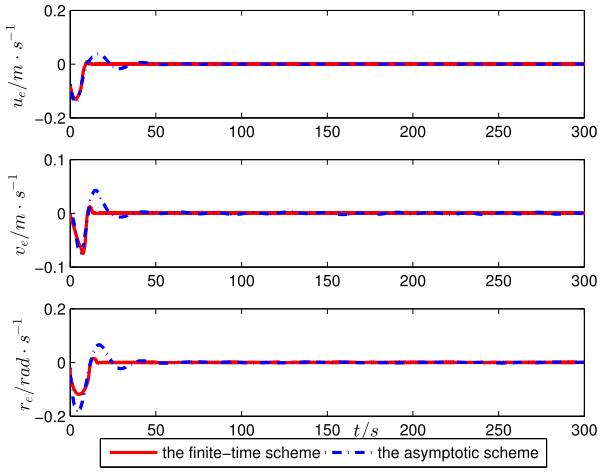

Fig. 10. The velocity tracking errors in the earth-fixed frame.

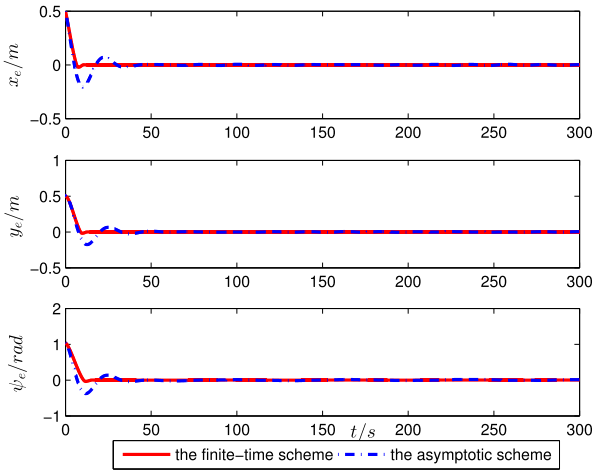

Fig. 11. The locations and yaw angle tracking errors.

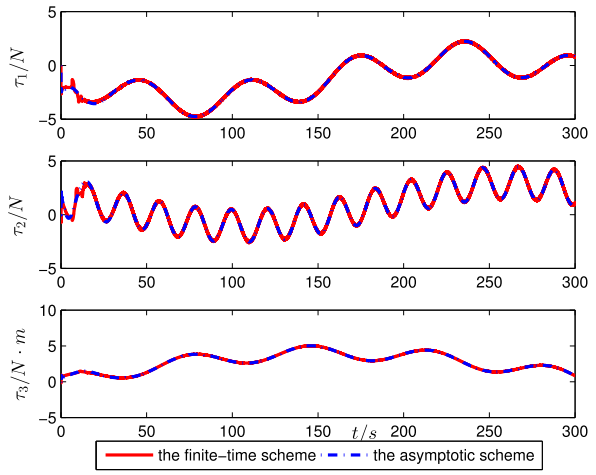

Fig. 12. The control inputs for both schemes.

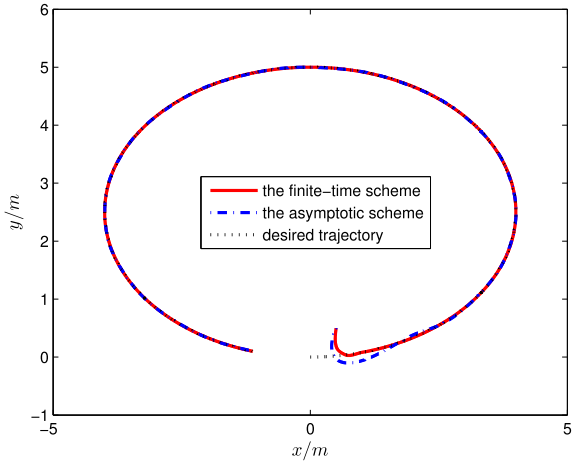

Fig. 13. The trajectories of two schemes in xy-plane.

further observed that the proposed scheme can make fast the vessel track the reference trajectory.

The quantitative analyses are listed in Table 2, where τ_{Rob} is originated from the proposed scheme without the estimated lumped disturbances $\hat{\chi}$ to show the robustness. As shown in Table 2, the proposed control law $\tau_{(35)}$ under uncertainties and disturbance has better transient and steady state performance than τ_{asy}. Meanwhile, the robustness is greatly enhanced due to the introduction of the FXESO. In Table 2, for the trajectory tracking, the settling time means the response curve reaching and staying within a range of certain percentage (usually 5% or 2%) of the final value (Tay et al., 1998). In this paper, the 2% error bounds can be selected so as to verify the superiority and effectiveness.

5.2. The point stabilization performance comparisons

In the simulations, the point stabilization control law (35) will be taken into account. The initial and desired values are respectively selected as $\eta(0) = [20\ \text{m}, 20\ \text{m}, \pi/18\ \text{rad}]^T$, $\eta_d = [0\ \text{m}, 0\ \text{m}, 0\ \text{rad}]^T$. The design parameters, gains and lumped disturbances for the observer and controller are same as the counterparts in the first case of Section 5.1.

Simulation comparison results are shown in Figs. 14–19. As depicted in Figs. 14–16, the proposed control law (35) guarantees the MSV can converge to the origin in a better transient performance, which is critical for the entire control system. In comparison with the control inputs in Figs. 17 and 18, the proposed scheme does not consume too much energy and not easily give rise to the input saturation in the initial phase. The two motion trajectories in xy-plane are depicted in Fig. 19.

Table 2
Performance indices comparisons of controllers.

Controller	$\tau_{(19)}$	τ_{asym}	τ_{Rob}
Settling time t_s	13.59	68.33	–
$\int_0^{t_{final}} \lvert u_e \rvert dt$	0.8362	1.4795	29.3328
$\int_0^{t_{final}} \lvert v_e \rvert dt$	0.4588	1.0588	31.4150
$\int_0^{t_{final}} \lvert r_e \rvert dt$	1.1279	2.3953	196.7376
$\int_0^{t_{final}} \lvert x_e \rvert dt$	1.5819	4.2952	77.8121
$\int_0^{t_{final}} \lvert y_e \rvert dt$	2.4365	4.9472	79.4298
$\int_0^{t_{final}} \lvert \psi_e \rvert dt$	5.7150	10.4951	28859.2058
$\int_0^{t_{final}} t \lvert u_e \rvert dt$	3.8684	25.7406	4427.6710
$\int_0^{t_{final}} t \lvert v_e \rvert dt$	3.5848	53.9381	4261.9381
$\int_0^{t_{final}} t \lvert r_e \rvert dt$	6.9807	60.7755	29852.6045
$\int_0^{t_{final}} t \lvert x_e \rvert dt$	3.5921	151.2276	8578.3322
$\int_0^{t_{final}} t \lvert y_e \rvert dt$	7.3830	146.7401	7529.2730
$\int_0^{t_{final}} t \lvert \psi_e \rvert dt$	20.3892	448.6183	6099730.9336

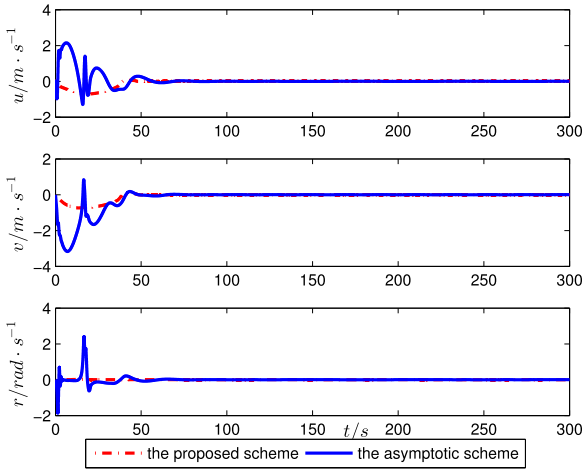

Fig. 14. The velocities for two schemes in the body-fixed frame.

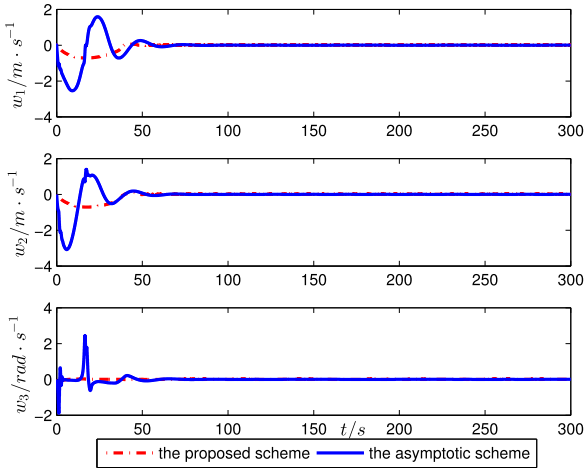

Fig. 15. The velocities for two schemes in the earth-fixed frame.

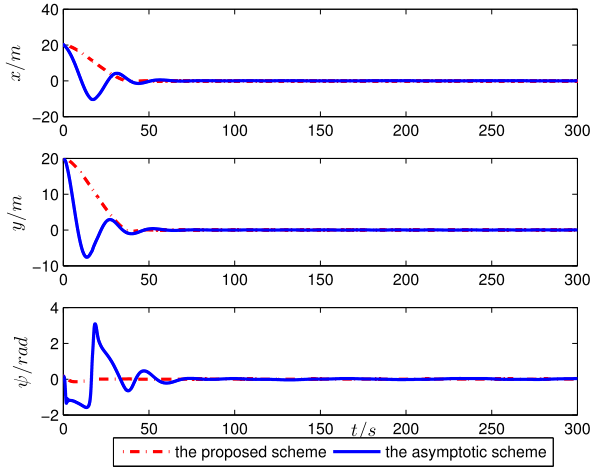

Fig. 16. The locations and yaw angle.

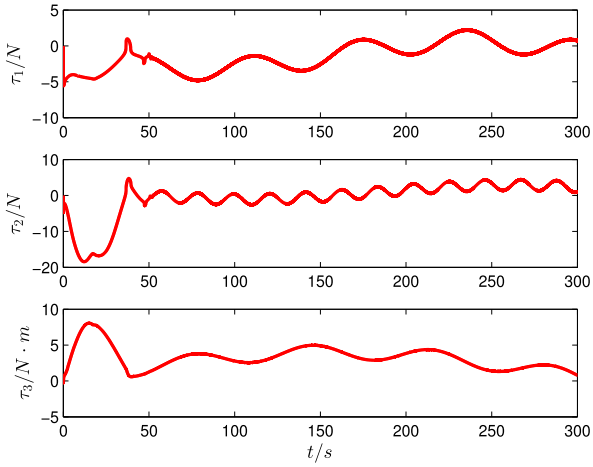

Fig. 17. The control inputs of the proposed scheme.

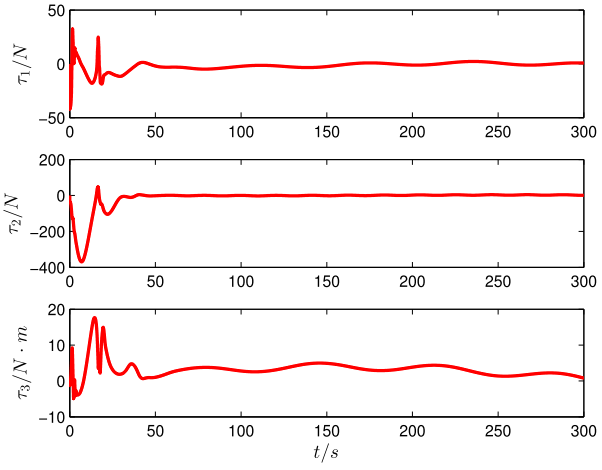

Fig. 18. The control inputs of the asymptotic scheme.

6. Conclusions

In this paper, a novel output feedback control scheme has been proposed for an MSV. By virtue of the FXESO and FHC methods, the proposed scheme can guarantee an MSV to precisely track the desired trajectory subject to uncertainties, unknown external disturbances and unmeasured velocities. By comparing with the FTESO and LESO, the proposed FXESO can achieve desirable performance. As shown in the simulations and Tables 1–2, the proposed scheme is superior to the asymptotic one in convergence rate and accuracy. Meanwhile, under the same control framework, the point stabilization can also make the remarkable performance. In the future works, an underactuated MSV

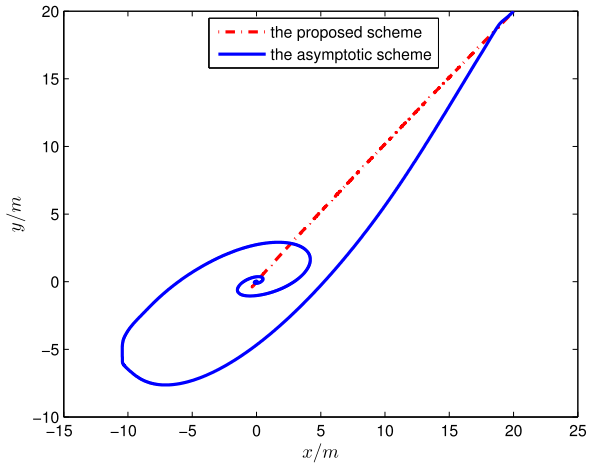

Fig. 19. The trajectories of two schemes in *xy*-plane.

and actuator saturation will be considered into the proposed scheme based on sampling step, small delays and sampling noise.

Acknowledgments

This work was supported by the National Natural Science Foundation of China (51809113), Natural Science Foundation of Liaoning Province, China (20180520036) and Fundamental Research Funds for the Central Universities of China (3132018129).

References

Basin, M., Yu, P., Shtessel, Y., 2016. Finite- and fixed-time differentiators utilising HOSM techniques. IET Control Theory Appl. 11 (8), 1144–1152.

Basin, M.V., Yu, P., Shtessel, Y.B., 2017. Hypersonic missile adaptive sliding mode control using finite- and fixed-time observers. IEEE Trans. Ind. Electron. 65 (1), 930–941.

Behal, A., Dawson, D.M., Dixon, W.E., Fang, Y., 2002. Tracking and regulation control of an underactuated surface vessel with nonintegrable dynamics. IEEE Trans. Automat. Control 47 (3), 495–500.

Cui, R., Chen, L., Yang, C., Chen, M., 2017a. Extended state observer-based integral sliding mode control for an underwater robot with unknown disturbances and uncertain nonlinearities. IEEE Trans. Ind. Electron. 64 (8), 6785–6795.

Cui, R., Ge, S.S., How, B.V.E., Choo, Y.S., 2010. Leader-follower formation control of underactuated autonomous underwater vehicles. Ocean Eng. 37 (17), 1491–1502.

Cui, R., Li, Y., Yan, W., 2016a. Mutual information-based multi-AUV path planning for scalar field sampling using multidimensional RRT. IEEE Trans. Syst. Man Cybern. Syst. 46 (7), 993–1004.

Cui, R., Yang, C., Li, Y., Sharma, S., 2017b. Adaptive neural network control of AUVs with control input nonlinearities using reinforcement learning. IEEE Trans. Syst. Man Cybern. Syst. 47 (6), 1019–1029.

Cui, R., Zhang, X., Cui, D., 2016b. Adaptive sliding-mode attitude control for autonomous underwater vehicles with input nonlinearities. Ocean Eng. 123, 45–54.

Dai, Y., Yu, S., 2018. Design of an indirect adaptive controller for the trajectory tracking of UVMS. Ocean Eng. 151, 234–245.

Ding, S., Chen, W., Mei, K., Murray-smith, D., 2019. Disturbance observer design for nonlinear systems represented by input–output models. IEEE Trans. Ind. Electron. http://dx.doi.org/10.1109/TIE.2019.2898585.

Do, K.D., 2016. Global robust adaptive path-tracking control of underactuated ships under stochastic disturbances. Ocean Eng. 111, 267–278.

Du, H., Li, S., 2012. Finite-time attitude stabilization for a spacecraft using homogeneous method. J. Guid. Control Dyn. 35 (3), 740–748.

Fossen, T.I., 2002. Marine Control Systems: Guidance, Navigation, and Control of Ships, Rigs and Underwater Vehicles.

Fu, M., Yu, L., 2018. Finite-time extended state observer-based distributed formation control for marine surface vehicles with input saturation and disturbances. Ocean Eng. 159, 219–227.

Hall, C.E., Shtessel, Y.B., 2006. Sliding mode disturbance observer-based control for a reusable launch vehicle. J. Guid. Control Dyn. 29 (6), 1315–1328.

Hong, Y., Xu, Y., Huang, J., 2002. Finite-time control for robot manipulators. Syst. Control Lett. 46 (4), 243–253.

Huang, Y., Zhu, M., Zheng, Z., Feroskhan, M., 2019. Fixed-time autonomous shipboard landing control of a helicopter with external disturbances. Aerosp. Sci. Technol. 84, 18–30.

Li, S., Sun, H., Yang, J., Yu, X., 2015. Continuous finite-time output regulation for disturbed systems under mismatching condition. IEEE Trans. Automat. Control 60 (1), 277–282.

Liu, S., Liu, Y., Wang, N., 2017. Robust adaptive self-organizing neuro-fuzzy tracking control of UUV with system uncertainties and unknown deadzone nonlinearity. Nonlinear Dynam. 89 (2), 1397–1414.

Liu, L., Wang, D., Peng, Z., 2015. Direct and composite iterative neural control for cooperative dynamic positioning of marine surface vessels. Nonlinear Dynam. 81 (3), 1315–1328.

Ni, J., Liu, L., Chen, M., Liu, C., 2018. Fixed-time disturbance observer design for brunovsky systems. IEEE Trans. Circuits Syst. Express Briefs 65 (3), 341–345.

Peng, Z., Wang, D., Chen, Z., Hu, X., Lan, W., 2013. Adaptive dynamic surface control for formations of autonomous surface vehicles with uncertain dynamics. IEEE Trans. Control Syst. Technol. 21 (2), 513–520.

Qu, Y., Xiao, B., Fu, Z., 2018. Trajectory exponential tracking control of unmanned surface ships with external disturbance and system uncertainties. ISA Trans. 78, 47–55.

Shi, Y., Shen, C., Fang, H., Li, H., 2017. Advanced control in marine mechatronic systems: a survey. IEEE/ASME Trans. Mechatron. 22 (3), 1121–1131.

Srensen, A.J., 2011. A survey of dynamic positioning control systems. Annu. Rev. Control 35 (1), 123–136.

Sun, J., Yi, J., Pu, Z., Tan, X., 2018. Fixed-time sliding mode disturbance observer-based nonsmooth backstepping control for hypersonic vehicles. IEEE Trans. Syst. Man Cybern. Syst http://dx.doi.org/10.1109/TSMC.2018.2847706.

Tay, T.T., Mareels, I., Moore, J.B., 1998. High Performance Control. Birkhuser, Boston.

Tian, B., Zuo, Z., Yan, X., Wang, H., 2017. Fixed-time output feedback control scheme for double integrator systems. Automatica 80, 17–24.

Tran, X.T., Kang, H.J., 2015. A novel adaptive finite-time control method for a class of uncertain nonlinear systems. Int. J. Precis. Eng. Manuf. 16 (13), 2647–2654.

Wang, N., Lv, S., Meng, J.E., Chen, W.H., 2017a. Fast and accurate trajectory tracking control of an autonomous surface vehicle with unmodeled dynamics and disturbances. IEEE Trans. Intell. Veh. 1 (3), 230–243.

Wang, N., Lv, S., Zhang, W., Liu, Z., Er, M.J., 2017b. Finite-time observer based accurate tracking control of a marine vehicle with complex unknowns. Ocean Eng. 145 (15), 406–415.

Wang, N., Qian, C., Sun, J.C., Liu, Y.C., 2016. Adaptive robust finite-time trajectory tracking control of fully actuated marine surface vehicles. IEEE Trans. Control Syst. Technol. 24 (4), 1454–1462.

Xiang, X., Yu, X., Lapierre, L., Zhang, J., Zhang, Q., 2017. Survey on fuzzy-logic based guidance and control of marine surface vehicles and underwater vehicles. Int. J. Fuzzy Syst. 20 (2), 572–586.

Yan, Z., Wang, J., 2012. Model predictive control for tracking of underactuated vessels based on recurrent neural networks. IEEE J. Ocean. Eng. 37 (4), 717–726.

Yan, Y., Yu, S., 2018. Sliding mode tracking control of autonomous underwater vehicles with the effect of quantization. Ocean Eng. 151, 322–328.

Yang, Y., Du, J., Liu, H., Guo, C., 2014. A trajectory tracking robust controller of surface vessels with disturbance uncertainties. IEEE Trans. Control Syst. Technol. 22 (4), 1511–1518.

Yang, T., Yu, S., Yan, Y., 2019. Formation control of multiple underwater vehicles subject to communication faults and uncertainties. Appl. Ocean Res. 82, 109–116.

Yu, X., Li, P., Zhang, Y., 2018. The design of fixed-time observer and finite-time fault-tolerant control for hypersonic gliding vehicles. IEEE Trans. Ind. Electron. 65 (5), 4135–4144.

Yu, S., Long, X., 2015. Finite-time consensus for second-order multi-agent systems with disturbances by integral sliding mode. Automatica 54, 158–165.

Yu, C., Xiang, X., Lapierre, L., Zhang, Q., 2017. Nonlinear guidance and fuzzy control for three-dimensional path following of an underactuated autonomous underwater vehicle. Ocean Eng. 146 (1), 457–467.

Yu, S., Yu, X., Shirinzadeh, B., Man, Z., 2005. Continuous finite-time control for robotic manipulators with terminal sliding mode. Automatica 41 (11), 1957–1964.

Yu, R., Zhu, Q., Xia, G., Liu, Z., 2012. Sliding mode tracking control of an underactuated surface vessel. IET Control Theory Appl. 6 (3), 461–466.

Zhang, L., Wei, C., Wu, R., Cui, N., 2018. Fixed-time extended state observer based non-singular fast terminal sliding mode control for a VTVL reusable launch vehicle. Aerosp. Sci. Technol. 82–83 (16), 70–79.

Zhang, J., Yu, S., Yan, Y., 2019. Fixed-time output feedback trajectory tracking control of marine surface vessels subject to unknown external disturbances and uncertainties. ISA Trans. http://dx.doi.org/10.1016/j.isatra.2019.03.007.

Zhang, G., Zhang, X., 2014. Concise robust adaptive path-following control of underactuated ships using DSC and MLP. IEEE J. Ocean. Eng. 39 (4), 685–694.

Zhao, L., Zhang, B., Yang, H., Wang, Y., 2017. Finite-time tracking control for pneumatic servo system via extended state observer. IET Control Theory Appl. 11 (16), 2808–2816.